Toroidal dipolar excitation and macroscopic electromagnetic properties of metamaterials

V. Savinov,[1,*] V. A. Fedotov,[1] and N. I. Zheludev[1,2]

[1]*Optoelectronics Research Centre & Centre for Photonic Metamaterials, University of Southampton,*
Southampton SO17 1BJ, United Kingdom
[2]*Centre for Disruptive Photonic Technologies, Nanyang Technological University, Singapore 637371, Singapore*

The toroidal dipole is a peculiar electromagnetic excitation that can not be presented in terms of standard electric and magnetic multipoles. A static toroidal dipole has been shown to lead to violation of parity in atomic spectra and many other unusual electromagnetic phenomena. The existence of electromagnetic resonances of toroidal nature was experimentally demonstrated only recently, first in the microwave metamaterials, and then at optical frequencies, where they could be important in spectroscopy analysis of a wide class of media with constituents of toroidal symmetry, such as complex organic molecules, fullerenes, bacteriophages, etc. Despite the experimental progress in studying toroidal resonances, no direct link has yet been established between microscopic toroidal excitations and macroscopic scattering characteristics of the medium. To address this essential gap in the electromagnetic theory, we have developed an analytical approach for calculating the transmissivity and reflectivity of thin slabs of materials that exhibit toroidal dipolar excitations.

I. INTRODUCTION

The toroidal dipole, shown in Fig. 1, is the first member of the family of toroidal multipoles [1–3]. It was discovered by Zel'dovich [4] in 1957, and has since been linked to parity nonconservation in the atomic spectra [5–7] and was shown to lead to the violation of Newton's third law [8]. A combination of the colocated electric and toroidal dipoles can result in the so-called nontrivial nonradiating configuration (also known as the "anapole moment" [9]) that emits vector and scalar potential without emitting electromagnetic radiation [9–11]. Different opinions exist on whether such nonradiating configuration could allow observation of the time-dependent Aharonov-Bohm effect [9,12].

Due to complexity of the current distribution that induces the toroidal dipole excitation (see Fig. 1), the toroidal dipole moment can only arise in the highly confined high-quality resonant modes of the subwavelength scatterers. Consequently, the study of toroidal dipole excitations could have significant repercussions for plasmonic scatterers with high-quality response, such as surface plasmon sensors [13–15], nanolasers [16], and metallic nanoparticles for nonlinear optics [17–22].

Despite its intriguing properties, the toroidal dipole is usually omitted in literature on classical electrodynamics [23,24]. Such omission is not justified since, while the radiation from any subwavelength charge-current distribution can be expanded in terms of just the electric and magnetic multipole fields, all three multipole families (including the toroidal multipoles) will be required for a complete expansion of the charge-current distribution itself [2]. The importance of accounting for the toroidal multipoles has recently been demonstrated with the experimental observation of toroidal dipole excitations in a microwave metamaterial [25], followed by further observations at microwave [11,26,27] and at optical frequencies [28–32]. This calls for the development of a

theory that links the microscopic toroidal excitations to the macroscopic response of the material, i.e., the transmission and reflection. In this paper, we develop a fully analytical formalism, which addresses this issue.

II. RADIATION FROM AN INFINITE PLANAR ARRAY OF ARBITRARY SUBWAVELENGTH EMITTERS

The electromagnetic properties of media are usually described in terms of macroscopic material parameters (e.g., dielectric permittivity and magnetic permeability), which, through homogenization of Maxwell's equations, establish a connection between media's macroscopic electromagnetic response and microscopic charge-current excitations induced in media's constituents, i.e. atoms or molecules [23]. Most homogenization schemes only consider the conventional electric and magnetic multipole excitations, but the modifications that arise with the inclusion of toroidal dipoles have also been discussed [33,34]. Such effective medium description is being also applied to the metamaterials, man-made material composites with exotic electromagnetic properties achieved through structuring on the subwavelength scale [35–37]. However, obtaining effective material parameters for the metamaterials is not straightforward and often difficult due to their structural inhomogeneity and strong spatial dispersion [38,39].

An alternative route, developed in this work, lies in relating the multipolar decomposition of the microscopic charge-current excitations, within the unit cell of the electromagnetic medium, directly to the transmission and reflection of that medium. Our approach is particularly suited for two-dimensional metamaterials, as well as for films of subwavelength thickness made from conventional materials. A similar problem of calculating the scattered radiation from arrays of metallic resonators has been addressed in the past using the fast multipole method (FMM) [40–44], and periodic Green's functions for the Helmholtz equation [45–47]. What makes our approach different is that it yields expressions sufficiently compact to be suitable not only for computer-aided
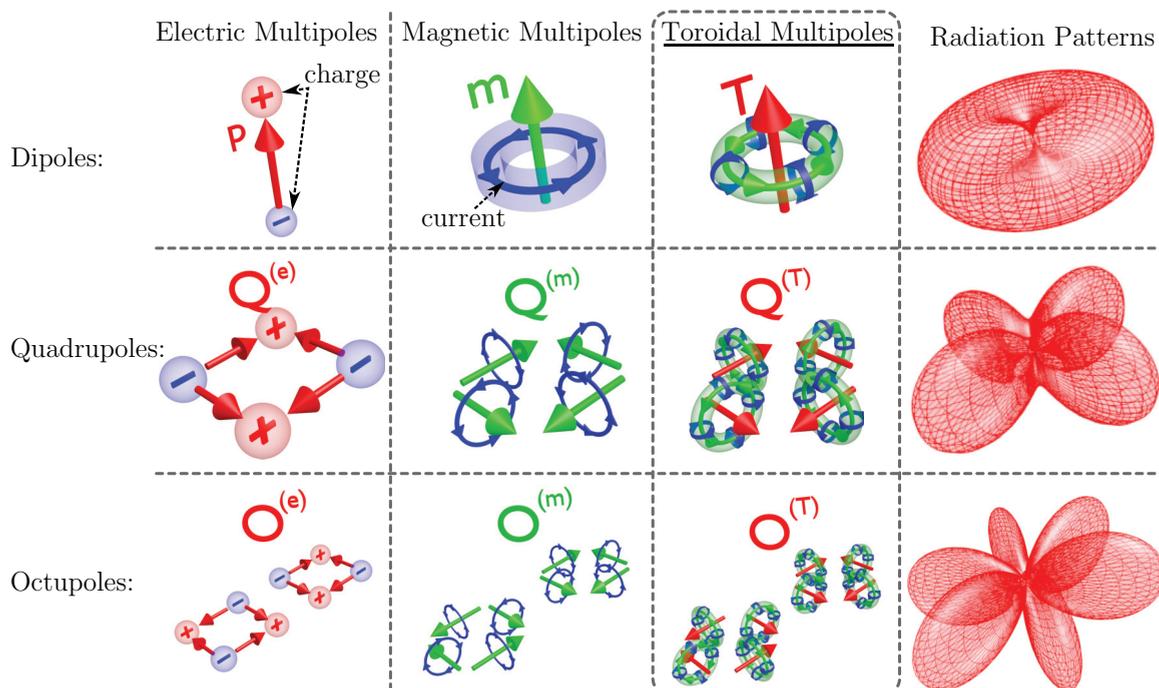
_____
*vs1106@orc.soton.ac.uk

FIG. 1. (Color online) Three families of dynamic multipoles. The three columns on the left show the charge-current distributions that give rise to the electric (**p**), magnetic (**m**), and toroidal (**T**) dipoles, electric ($\mathbf{Q}^{(\mathbf{e})}$), magnetic ($\mathbf{Q}^{(\mathbf{m})}$), and toroidal ($\mathbf{Q}^{(\mathbf{T})}$) quadrupoles, as well as the electric ($\mathbf{O}^{(\mathbf{e})}$), magnetic ($\mathbf{O}^{(\mathbf{m})}$), and toroidal ($\mathbf{O}^{(\mathbf{T})}$) octupoles. The toroidal dipole (**T**) is created by the oscillating poloidal current, the current that flows along the meridians of a torus. The next member of the toroidal multipole family, the toroidal quadrupole ($\mathbf{Q}^{(\mathbf{T})}$), is created by the antialigned pairs of toroidal dipoles. The toroidal octupole ($\mathbf{O}^{(\mathbf{T})}$), in turn, is created by antialigned toroidal quadrupoles. The column on the right shows the patterns of radiation (i.e., intensity as a function of direction) emitted by the various harmonically oscillating multipoles (for quadrupoles, only the radiation associated with the off-diagonal component of the second-rank quadrupole moment tensor is shown, for octupoles only the radiation associated with the component of the third-rank octupole moment tensor, with two repeated indices and the third distinct index, is shown).

calculations (like FMM), but also for the purely analytic evaluation. At the same time, our approach accounts not only for the conventional multipoles, but also for the elusive toroidal multipoles (see Fig. 1). By applying the derived formalism to a test-case study metamaterial, we show that characterization of the electromagnetic response of a certain class of structures is greatly enhanced by taking the toroidal multipoles into account.

We will now proceed to deriving a general expression for the electromagnetic field scattered by a two-dimensional subwavelength array of identical charge-current excitations that are represented by a finite series of dynamic multipoles. For the case of passive materials (and metamaterials), these multipoles will have been induced by normally incident plane-wave radiation. We assume that the multipole moments can either be extracted from the numerical simulation of the induced currents, or calculated from the dynamics of charge and current densities anticipated for the metamolecules of a known geometry [48–52]. In the interest of brevity, only the key steps of the derivation will be demonstrated, yielding the expression for the radiation from a two-dimensional array of toroidal dipoles, before giving the full expression that includes all leading multipoles.

We start from the far-field distribution of the electric field radiated by a single oscillating toroidal dipole, which has been derived by Radescu and Vaman in Ref. [2]

[Eq. (3.15)]:

$$\mathbf{E}(\mathbf{r}) = \frac{-i\mu_0 c^2 k^3}{3\sqrt{2\pi}} \frac{\exp(-ikr)}{r}$$
$$\times \sum_{m=0,\pm 1} T_{1m}[\mathbf{Y}_{1,2,m} + \sqrt{2}\mathbf{Y}_{1,0,m}], \qquad (1)$$

$$T_{1,\pm 1} = \frac{1}{\sqrt{2}}(\mp T_x + iT_y), \qquad (2)$$

$$T_{1,0} = T_z, \qquad (3)$$

$$\mathbf{T} = \frac{1}{10c} \int d^3r \, [\mathbf{r}(\mathbf{r} \cdot \mathbf{J}) - 2r^2\mathbf{J}]. \qquad (4)$$

Here, μ_0 is the magnetic permeability of vacuum, c is the speed of light, **r** is the vector connecting the location of the dipole with the observer, and $\mathbf{Y}_{l,l',m}$ are the spherical vector harmonics that allow us to represent any vector field on the surface of the unit sphere in the same way as spherical harmonics allow us to represent any scalar field on the surface of the unit sphere [1,2,53]. The toroidal dipole moment is denoted by **T**, while **J** is the current density that gives rise to such dipole. Unlike Vaman and Radescu [2], we are using the SI units and assume harmonic time dependence specified by $\exp(+i\omega t)$, where ω is the angular frequency and $k = 2\pi/\lambda = \omega/c$ is the wave number.
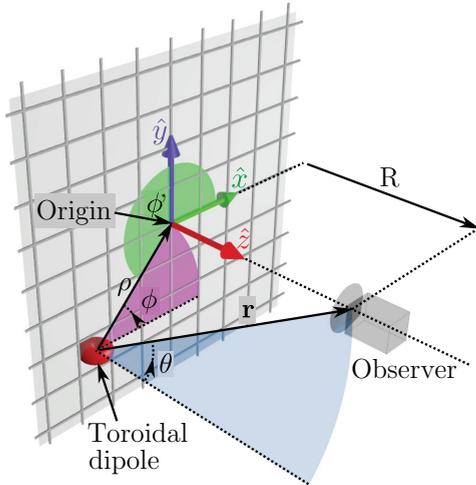
FIG. 2. (Color online) Calculating scattering from a two-dimensional planar array of toroidal dipoles. A single toroidal dipole is represented by its radiation pattern. The vectors connecting the dipole to the observer and to the origin of the array are $\mathbf{r}$ and ρ, respectively. The observer is located at distance R from the array. The vector $\mathbf{R}$ is perpendicular to the array plane. The position of the observer relative to the dipole in spherical polar coordinates is (r, θ, ϕ). The position of the dipole relative to the origin of the array in cylindrical polar coordinates is (ρ, ϕ').

The total field radiated by an infinitely large planar array of toroidal dipoles ($\mathbf{E}_s$) is obtained by summing the contributions from all dipoles at the position of the observer. We assume that all dipoles oscillate in phase (i.e., the multipole array is induced by the plane wave at normal incidence), and that the unit cell of the array (separation between dipoles) is sufficiently smaller than the wavelength of incident radiation. The latter assumption allows us to replace the sum over the unit cells with an integral over the array area [Δ^2 denotes the area of the unit cell; see Appendix F for the justification of Eq. (5)]:

$$\mathbf{E_s} = \sum_{\mathbf{r}} \mathbf{E(r)} \approx \frac{1}{\Delta^2} \int_{\text{array}} d^2 r \, \mathbf{E(r)}. \qquad (5)$$

We choose to work in the coordinate system where the array of dipoles lies in the xy plane and the incident/scattered radiation propagates along the z axis (see Fig. 2). Explicit evaluation of the relevant spherical vector harmonics [2] results in

$$\mathbf{Y}_{1,2,\pm 1} + \sqrt{2}\mathbf{Y}_{1,0,\pm 1}$$
$$= \begin{pmatrix} \pm\sqrt{\frac{3}{10}}Y_{2,\pm 2} \mp \sqrt{\frac{1}{20}}Y_{2,0} \mp Y_{0,0} \\ -i\sqrt{\frac{3}{10}}Y_{2,\pm 2} - i\sqrt{\frac{1}{20}}Y_{2,0} - iY_{0,0} \\ -\sqrt{\frac{3}{10}}Y_{2,\pm 1} \end{pmatrix},$$

$$\mathbf{Y}_{1,2,0} + \sqrt{2}\mathbf{Y}_{1,0,0} = \begin{pmatrix} \sqrt{\frac{3}{20}}Y_{2,1} - \sqrt{\frac{3}{20}}Y_{2,-1} \\ -i\sqrt{\frac{3}{20}}Y_{2,1} - i\sqrt{\frac{3}{20}}Y_{2,-1} \\ -\sqrt{\frac{2}{5}}Y_{2,0} + \sqrt{2}Y_{0,0} \end{pmatrix}.$$

The vectors are presented in the Cartesian basis with column entries indicating the x, y, and z components (from top to bottom, respectively), $Y_{l,m}$ are the standard spherical harmonics [2]. The basic integral that needs to be evaluated in Eq. (5), after substitution of Eq. (1), is ($l = 1, 2, 3, \ldots$; m is integer and $-l \leqslant m \leqslant l$):

$$I_{l,m} = \int d^2 r \, Y_{l,m} \exp(-ikr)/r. \qquad (6)$$

Equation (6) can be rewritten as (see Appendix A)

$$I_{l,m} = \int_0^{2\pi} d\phi' \int_0^{\infty} \rho \, d\rho \, Y_{l,m}(\theta, \phi' + \pi) \exp(-ikr)/r, \quad (7)$$

where ρ and ϕ' are the radius and the angle specifying the position of the toroidal dipoles in the planar array (over which the integration is carried out), r is the distance between the observer and the toroidal dipole, θ is the angle between the line connecting the observer to a toroidal dipole and a normal to the array, and R is the distance from the observer to the array. All variables are annotated in Fig. 2. The unit vector pointing from the array towards the observer is $\hat{\mathbf{R}} = \mathbf{R}/R$.

By assuming that the propagation of radiation occurs in a space with losses (i.e., negative imaginary part of k; losses can be marginally small) and by concentrating only on the far-field component of the radiation ($R \gg \lambda$), one can show that (see Appendix A)

$$I_{l,m} \cong \frac{\pi \delta_{m,0}(\hat{\mathbf{R}} \cdot \hat{\mathbf{z}})^l}{ik}\sqrt{\frac{2l+1}{\pi}}\exp(-ikR). \qquad (8)$$

Substitution of Eq. (1) into Eq. (5) and use of Eq. (8) allows us to derive

$$\mathbf{E_s} = \frac{\mu_0 c^2 k^2}{4\Delta^2}\sqrt{2}\begin{pmatrix} T_{1,1} - T_{1,-1} \\ i(T_{1,1} + T_{1,-1}) \\ 0 \end{pmatrix}\exp(-ikR).$$

Further simplification produces the final form

$$\mathbf{E_s} = -\frac{\mu_0 c^2 k^2}{2\Delta^2}\mathbf{T}_{\parallel}\exp(-ikR). \qquad (9)$$

The subscript $(\ldots)_{\parallel}$ denotes the projection of the vector into the plane of the array. If one assumes the coordinate system shown in Fig. 2, where the array lies in the xy plane, the projection of the toroidal dipole is given by $\mathbf{T}_{\parallel} = T_x\hat{\mathbf{x}} + T_y\hat{\mathbf{y}}$ (i.e., the z component is dropped since it is perpendicular to the array). In general, $\mathbf{T}_{\parallel} = \mathbf{T} - (\mathbf{T} \cdot \hat{\mathbf{R}})\hat{\mathbf{R}}$.

Starting with the far-field distributions for other isolated multipoles (given in Appendix B) and repeating the derivation steps given above results in

$$\begin{aligned}
\mathbf{E}_s = \frac{\mu_0 c^2}{2\Delta^2}\bigg\{ &-ik\mathbf{p}_{\parallel} + ik\hat{\mathbf{R}}\times\left(\mathbf{m}_{\parallel} - \frac{k^2}{10}\mathbf{m}_{\parallel}^{(1)}\right) \\
&-k^2\left(\mathbf{T}_{\parallel} + \frac{k^2}{10}\mathbf{T}_{\parallel}^{(1)}\right) + k^2(\mathbf{Q}^{(\mathbf{e})}\cdot\hat{\mathbf{R}})_{\parallel} \\
&-\frac{k^2}{2}\hat{\mathbf{R}}\times(\mathbf{Q}^{(\mathbf{m})}\cdot\hat{\mathbf{R}})_{\parallel} - \frac{ik^3}{3}(\mathbf{Q}^{(\mathbf{T})}\cdot\hat{\mathbf{R}})_{\parallel} \\
&+ik^3[(\mathbf{O}^{(\mathbf{e})}\cdot\hat{\mathbf{R}})\cdot\hat{\mathbf{R}}]_{\parallel} - \frac{ik^3}{180}\hat{\mathbf{R}}\times[(\mathbf{O}^{(\mathbf{m})}\cdot\hat{\mathbf{R}})\cdot\hat{\mathbf{R}}]_{\parallel}\bigg\} \\
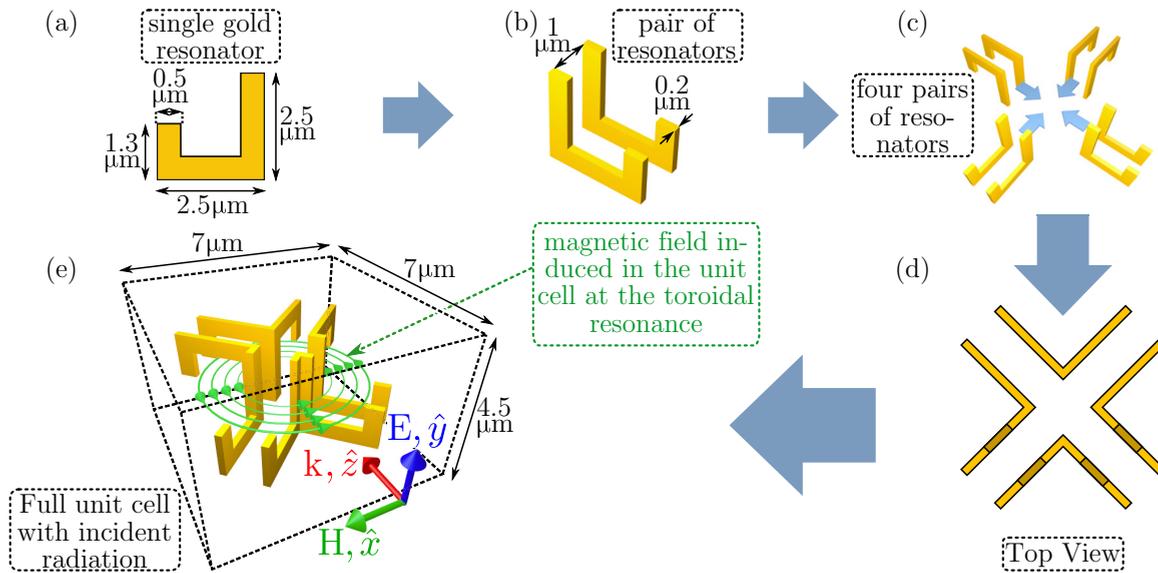&\times\exp(-ikR).
\end{aligned} \qquad (10)$$

FIG. 3. (Color online) The design of the unit cell of the test-case toroidal metamaterial. (a) The most basic building block of the unit cell. An L-shaped resonator out of gold. (b) The L-shaped resonators are put in pairs with 1-μm separation between them. (c), (d) Four pairs of resonators are combined to make a single large resonator. The two pairs of resonators at the front end are oriented in the usual way [same as in (a) and (b), with the split pointing up], the two pairs of resonators at the rear end are turned upside down. (e) The full unit cell which consists of the large gold resonator at the center embedded into the SU-8 polymer. The metamaterial is created by translating and replicating the unit cell along the x and y axes. The metamaterial is driven by the plane-wave radiation propagating along the $\hat{\mathbf{z}}$ axis and polarized along the $\hat{\mathbf{y}}$ axis. The configuration of the magnetic field that gives rise to the toroidal dipole excitation in the metamaterial is schematically illustrated with green field lines.

Equation (10) allows us to calculate the electric field emitted by an infinitely large two-dimensional array of metamolecules (or any subwavelength emitters), provided the induced charge-current density oscillations can be approximated by the first eight dynamic multipoles. The terms that contribute to the emitted field in Eq. (10) are the electric (**p**), magnetic (**m**), and toroidal (**T**) dipoles, electric ($\mathbf{Q^{(e)}}$), magnetic ($\mathbf{Q^{(m)}}$), and toroidal ($\mathbf{Q^{(T)}}$) quadrupoles, electric ($\mathbf{O^{(e)}}$) and magnetic ($\mathbf{O^{(m)}}$) octupoles, and the so-called mean-square radii of toroidal ($\mathbf{T}^{(1)}$) and magnetic ($\mathbf{m}^{(1)}$) dipoles, which are the lowest-order corrections retained to account for the finite size of the metamolecules [2]. The expressions used to calculate the multipole moments are given in Appendix C. Further multipole contributions to the radiation by an array of finite-size scatterers can be found in the same way.

III. MULTIPOLE DECOMPOSITION OF THE ELECTROMAGNETIC RESPONSE OF A TEST-CASE METAMATERIAL

Using Eq. (10), the radiation transmitted and reflected by the two-dimensional array of scatterers, under normal plane-wave illumination, can be found from

$$\mathbf{E}_{\text{reflected}} = [\mathbf{E}_s]_{\hat{\mathbf{R}}=-\hat{\mathbf{k}}},$$

$$\mathbf{E}_{\text{transmitted}} = [\mathbf{E}_s]_{\hat{\mathbf{R}}=\hat{\mathbf{k}}} + \mathbf{E}_{\text{incident}},$$

where $\hat{\mathbf{k}} = \mathbf{k}/k$ points in the direction of propagation of the incident radiation.

Next, we will apply our approach to study the electromagnetic response of a metamaterial designed to exhibit strong toroidal resonance in the mid-IR part of the spectrum. The unit

cell of the metamaterial array, shown in Fig. 3, contains a three-dimensional complex-shaped gold metamolecule immersed in the SU-8 polymer. The metamaterial design has been derived from the four-split-ring configuration proposed by Kaelberer *et al.* [25]. It has been heavily optimized for the novel metamaterial fabrication technique SAMPL [54], while trying to mitigate the effects of high Joule losses in the mid-IR range. We will omit the detailed description of the optimization procedure since the main purpose of this paper is to demonstrate that Eq. (10) provides a correct link between the macroscopic metamaterial response and the microscopic multipole excitations within the metamolecules even in the case of quite complex metamaterial design.

The transmission and reflection of the test-case metamaterial (Fig. 3) was simulated in the 14.5–23.5 μm range of wavelengths using full three-dimensional (3D) Maxwell's equations solver COMSOL MULTIPHYSICS 3.5a (see Appendix G for material constants used in simulations). The numerical model also provided data on spatial distribution of the conduction and displacement current density, which was used to calculate dynamic multipole moments induced in each metamolecule (see Appendix C).

The simulated transmission and reflection spectra are shown in Figs. 4(a) and 4(b) as solid curves, revealing two distinct resonances located at around 21.0 and 17.4 μm. The numerical spectra are very well matched by the results of the multipole calculations described above [see dashed curves in Fig. 4(a)]. Small discrepancies are attributed to somewhat limited accuracy of extracting the induced current distribution from the numerical model.

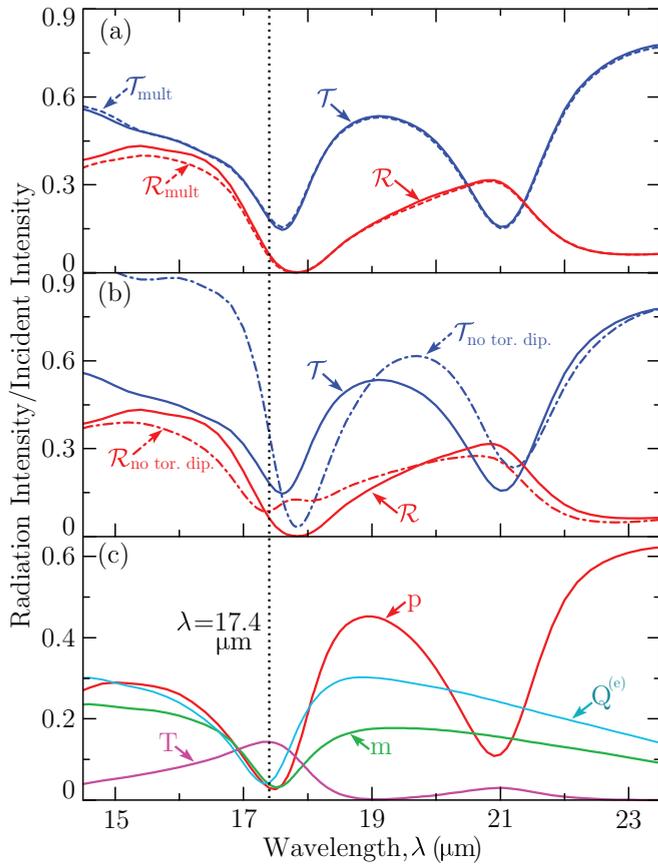The analysis of multipole scattering is presented in Fig. 4(c) (only four leading multipoles are shown, see

FIG. 4. (Color online) Electromagnetic response of the test-case toroidal metamaterial. The response of the metamaterial on Fig. 3 has been modeled using the realistic material constants for gold and SU-8 polymer (see Appendix G). (a) Transmission ($\mathcal{T}$; blue) and reflection ($\mathcal{R}$; red) of the metamaterial. The solid curves ($\mathcal{T}$, $\mathcal{R}$) are obtained directly from numerical solution of Maxwell's equations, dashed curves ($\mathcal{T}_{\text{mult}}$, $\mathcal{R}_{\text{mult}}$) are obtained using Eq. (10), from the multipole moment representation of each metamolecule of the metamaterial. (b) The comparison of the directly calculated metamaterial transmission and reflection ($\mathcal{T}$, $\mathcal{R}$; solid curves) to the response obtained from multipoles but without the contribution of toroidal dipole ($\mathcal{T}_{\text{no tor. dip.}}$, $\mathcal{R}_{\text{no tor. dip.}}$; dashed-dotted curves). (c) Intensity of the radiation scattered back (i.e., reflected) by each of four leading multipoles when placed in an array [**p** (electric dipole), **m** (magnetic dipole), **T** (toroidal dipole), **Q**$^{(e)}$ (electric quadrupole)]. The radiation intensity in all three plots is normalized with respect to incident radiation.

Appendix D for the full expansion). One can clearly see that at longer-wavelength resonance (21.0 μm), the metamaterial response is dominated by the electric quadrupole and magnetic dipole scattering, and thus this resonance will be of no interest for the following discussion. By contrast, at the shorter-wavelength resonance (17.4 μm), the metamaterial response is clearly dominated by the toroidal dipole scattering which is more than three times larger than the contribution due to any other (standard) multipole (see Appendix H for the corresponding magnetic field distribution). It is also interesting to note that the dominance of toroidal dipole response would be even more dominant if the metamaterial was excited with two coherent counterpropagating waves that created an electric

field antinode at the origin (as was done in Refs. [55,56]). In this case, due to odd parity, the electric quadrupole and magnetic dipole excitations would be suppressed leaving only the toroidal dipole to dominate the metamaterial response, with the next strongest multipole excitation (electric dipole) being five times weaker.

Figure 4(c) shows that the toroidal dipole excitation must play a key role in forming the metamaterial macroscopic response at the shorter-wavelength resonance (17.4 μm). This can be verified directly by ignoring the toroidal dipole moment in the multipole calculations of the transmission and reflection. As one can see from Fig. 4(b), the correct replication of the resonant features is simply not possible in the frame of the standard multipole expansion, and the notion of the toroidal dipole is thus crucial for the correct interpretation of metamaterial's macroscopic response.

IV. CONCLUSION

In conclusion, we developed a fully analytical formalism that allows calculating the transmission and reflection properties of thin sheets of metamaterials and material composites, based on the dynamic multipole decomposition, including the toroidal dipole, of charge-current densities induced in their structure by an incident electromagnetic wave. In addition to the derived formalism, we provided a case study which proved that the contribution of the toroidal dipole is crucial for the correct interpretation of the reflection and the transmission spectra of a certain class of metamaterials. Our findings demonstrate that the toroidal dipole may be dominant in the response of the electromagnetic media, and therefore can not be neglected simply as a high-order correction to the electric or magnetic multipoles.

APPENDIX A: INTEGRAL INVOLVING THE SPHERICAL HARMONICS: $I_{l,m}$

Here, we will derive Eqs. (7) and (8). At the core of the derivation lies the evaluation of the following integral:

$$\int_R^\infty dr \left(\frac{R}{r}\right)^q \exp(-ikr) \cong \frac{\exp(-ikR)}{ik}, \quad \text{Im}(k) < 0.$$

$$\text{(A1)}$$

The case $q = 0$ can be found by the direct integration. Higher-order cases can be evaluated by relating them to the exponential integrals. Abramowitz and Stegun [57] define the exponential integral as [Eq. (5.1.4) of Ref. [57]]

$$E_n(z) = \int_1^\infty dt \frac{\exp(-zt)}{t^n}, \quad n = 0, 1, 2, \ldots, \quad \text{Re}(z) > 0.$$

We are interested in the asymptotic expansion of the $E_n(z)$ for the case of large z given in Eq. (5.1.51) of Ref. [57]:

$$\lim_{z\to\infty} E_n(z) \cong \frac{\exp(-z)}{z}[1 - O(1/z)], \quad |\arg(z)| < \frac{3}{2}\pi.$$

Equation (A1) can therefore as be evaluated as follows:

$$\int_R^\infty dr \left(\frac{R}{r}\right)^q \exp(-ikr)$$
$$= RE_q(ikR)$$
$$\cong R\frac{\exp(-ikR)}{ikR}[1 - O(1/kR)].$$

Note that $\text{Im}(k) < 0$ implies $\text{Re}(ikR) > 0$ and $|\arg(ikR)| < \pi/2$. Up to order $O(1/kR)$ or, equivalently, up to $O(\lambda/R)$, the expression becomes

$$\int_R^\infty dr \left(\frac{R}{r}\right)^q \exp(-ikr) \cong \frac{\exp(-ikR)}{ik}.$$

We now turn our attention to Eq. (6):

$$I_{l,m} = \int d^2r\, Y_{l,m}(\theta,\phi) \exp(-ikr)/r.$$

The integration is understood to be over the area of the array of multipoles as shown in Fig. 2. The position of each multipole in the plane of the array is given by ρ, the distance between the center point of the array and the considered multipole, and ϕ' the angle between the x axis and the vector connecting the center point of the array and the multipole in question. There is also another angle ϕ that belongs together with r and θ and denotes the position of the observer relative to the multipole under consideration (see Fig. 2). It is convenient to place the origin of the multipole array directly below the observer. In this case, the relation between ϕ and ϕ' takes a simple form $\phi = \phi' + \pi$, up to a full rotation around 2π. Figure 5 helps to visualize the two angles. The same choice of origin establishes the relation $r^2 = \rho^2 + R^2$.

One can now rewrite the integral in a more accessible way:

$$I_{l,m} = \int_0^{2\pi} d\phi' \int_0^\infty \rho\, d\rho\, Y_{l,m}(\theta,\phi' + \pi) \frac{\exp(-ikr)}{r}.$$
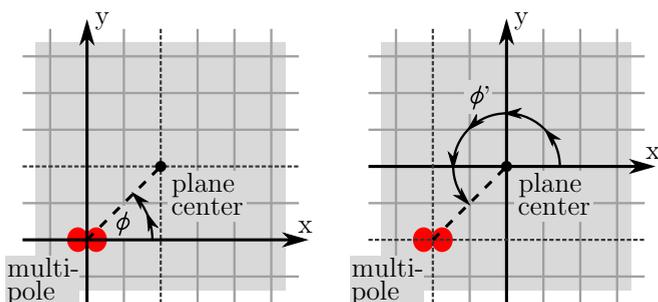

FIG. 5. (Color online) The difference between ϕ and ϕ'. Angle ϕ is defined in the coordinate frame of a multipole under consideration, while the angle ϕ' is defined in the coordinate frame of the multipole array (also see Fig. 2). The observer (see Fig. 2) is located directly above the origin of the array.

From $r^2 = \rho^2 + R^2$ it follows that $r\, dr = \rho\, d\rho$, so

$$I_{l,m} = \int_0^{2\pi} d\phi' \int_R^\infty r\, dr\, Y_{l,m}(\theta,\phi' + \pi)\frac{\exp(-ikr)}{r}$$
$$= (-1)^{m+m}\sqrt{\frac{2l+1}{4\pi}\frac{(l-m)!}{(l+m)!}}$$
$$\times \int d\phi' \exp(im\phi') \int_R^\infty dr\, P_l^m(\cos\theta) \exp(-ikr).$$

In the last step, we have expanded the spherical harmonic following the convention used by Arfken and Weber [58] (see Chap. 12.6), and substituted $\exp[im(\pi + \phi')] = (-1)^m \exp(im\phi')$. Here, the P_l^m denotes the associated Legendre functions. The expression above is simplified considerably by the fact that the integral over ϕ' is nonzero only for $m = 0$:

$$I_{l,m} = \pi\delta_{m,0}\sqrt{\frac{2l+1}{\pi}} \int_R^\infty dr\, P_l(\cos\theta) \exp(-ikr).$$

Above, we have used $P_l^0(x) = P_l(x)$ to replace the associated Legendre functions with Legendre polynomials (respectively). From Fig. 2 it follows that $\cos\theta = R/r$ for $\mathbf{R} = R\hat{\mathbf{z}}$, and $\cos\theta = -R/r$ for $\mathbf{R} = -R\hat{\mathbf{z}}$, thus $\cos\theta = (\hat{\mathbf{R}} \cdot \hat{\mathbf{z}}) \times R/r$. Using the parity property of Legendre polynomials [Eq. 12.37 in Ref. [58]] one obtains $P_l(\cos\theta) = (\hat{\mathbf{R}} \cdot \hat{\mathbf{z}})^l P_l(R/r)$. Being a polynomial, $P_l(x)$ can be expressed as power series $P_l(x) = \sum_{s=0}^\infty a_s^{(l)} x^s$, the integral then becomes [with use of Eq. (A1)]

$$I_{l,m} = \pi\delta_{m,0}\sqrt{\frac{2l+1}{\pi}}(\hat{\mathbf{R}} \cdot \hat{\mathbf{z}})^l$$
$$\times \sum_{s=0}^\infty a_s^{(l)} \int_R^\infty dr \left(\frac{R}{r}\right)^s \exp(-ikr)$$
$$\cong \pi\delta_{m,0}\sqrt{\frac{2l+1}{\pi}}(\hat{\mathbf{R}} \cdot \hat{\mathbf{z}})^l \sum_{s=0}^\infty a_s^{(l)}$$
$$\times \left(\frac{\exp(-ikR)}{ik} + O(\lambda/R)\right).$$

Finally, one uses the normalization of the Legendre polynomials to eliminate the sum: $P_l(1) = 1 = \sum_{s=0}^\infty a_s^{(l)}$ [Eq. (12.31) in Ref. [58]]. Thus,

$$I_{l,m} \cong \frac{\pi\delta_{m,0}(\hat{\mathbf{R}} \cdot \hat{\mathbf{z}})^l}{ik}\sqrt{\frac{2l+1}{\pi}} \exp(-ikR),$$

which completes the derivation.

APPENDIX B: MULTIPOLE DECOMPOSITION OF THE RADIATION FROM A LOCALIZED SOURCE

To derive the formula for the electric field radiated by the array of multipoles [see Eq. (10)], we have used the expression for the radiation emitted by the single multipole sources provided by Radescu and Vaman [2] [see Eq. (3.15) in particular]. Here, we will give the truncated series in the SI units and in the complex-valued time-harmonic approximation for the electric field emitted by the multipole sources.

Due to large number of terms, it is convenient to separate the series into different orders of l. The $l = 1$ subseries then

contains the dipolar contributions

$$\mathbf{E}_{(l=1)} \approx \frac{\mu_0 c^2}{3\sqrt{2\pi}} \frac{\exp(-ikr)}{r}$$
$$\times \sum_{m=0,\pm 1} \left[\left(k^2 Q_{1,m} - ik^3 T_{1,m} + ik^5 T_{1,m}^{(1)} \right) \right.$$
$$\times (\mathbf{Y}_{1,2,m} + \sqrt{2}\mathbf{Y}_{1,0,m})$$
$$\left. + i\sqrt{3} \left(k^2 M_{1,m} - k^4 M_{1,m}^{(1)} \right) \times \mathbf{Y}_{1,1,m} \right].$$

The $l=2$ subseries contains the quadrupolar contributions

$$\mathbf{E}_{(l=2)} \approx \frac{\mu_0 c^2}{10\sqrt{6\pi}} \frac{\exp(-ikr)}{r} \sum_{m=0,\pm 1,\pm 2} \left[\left(ik^3 Q_{2,m}^{(e)} + k^4 Q_{2,m}^{(T)} \right) \right.$$
$$\left. \times (\sqrt{2}\mathbf{Y}_{2,3,m} + \sqrt{3}\mathbf{Y}_{2,1,m}) - \sqrt{5}k^3 Q_{2,m}^{(m)}\mathbf{Y}_{2,2,m} \right].$$

The $l=3$ subseries contains the octupolar contributions

$$\mathbf{E}_{(l=3)} \approx -\frac{\mu_0 c^2 k^4}{15\sqrt{3\pi}} \frac{\exp(-ikr)}{r}$$
$$\times \sum_{m=0,\pm 1,\pm 2,\pm 3} \left[\frac{1}{7} O_{3,m}^{(e)}(\sqrt{3}\mathbf{Y}_{3,4,m} + 2\mathbf{Y}_{3,2,m}) \right.$$
$$\left. + \frac{i}{\sqrt{7}} O_{3,m}^{(m)}\mathbf{Y}_{3,3,m} \right].$$

The total field emitted is given by

$$\mathbf{E} = \mathbf{E}_{(l=1)} + \mathbf{E}_{(l=2)} + \mathbf{E}_{(l=3)} + (l > 3 \text{ subseries}).$$

Although the series given above are truncated at order k^4, the first-order correction for the toroidal dipole ($T_{1,m}^{(1)}$) of order k^5 is also included to avoid errors in the spectral range where toroidal dipole dominates (see Fig. 4). The other k^5 terms that can be included are the toroidal octupole, the electric and magnetic hexadecapoles ($l = 4$), and the first-order correction to the magnetic quadrupole.

One may notice that no correction terms for the electric dipoles have been included. Radescu and Vaman [2] have shown that the correction terms for the electric multipoles do not contribute to the far-field radiation emitted by arbitrary localized charge-current density distributions, while the correction terms for the magnetic and toroidal multipoles, by contrast, do contribute.

APPENDIX C: INTEGRALS FOR FINDING THE LEADING MULTIPOLES FROM A CURRENT DISTRIBUTION

The expressions we have used to calculate the multipole moments from the current density distribution are those given by Radescu and Vaman [2]. We will repeat them here for convenience. Note that the electric and magnetic multipoles are exactly the same as those given in the standard texts on electrodynamics [23] (apart from the different normalization constants).

Cartesian multipoles are computed by integrating over the charge density $\rho(\mathbf{r})$ or current density $\mathbf{J}(\mathbf{r})$ distribution within the unit cell ($\alpha,\beta,\gamma = x,y,z$):

$$p_\alpha = \int d^3r\, \rho\, r_\alpha = \frac{1}{i\omega} \int d^3r\, J_\alpha,$$

$$m_\alpha = \frac{1}{2c} \int d^3r\, [\mathbf{r} \times \mathbf{J}]_\alpha,$$

$$m_\alpha^{(1)} = \frac{1}{2c} \int d^3r\, [\mathbf{r} \times \mathbf{J}]_\alpha r^2,$$

$$T_\alpha = \frac{1}{10c} \int d^3r\, [(\mathbf{r} \cdot \mathbf{J})r_\alpha - 2r^2 J_\alpha],$$

$$T_\alpha^{(1)} = \frac{1}{28c} \int d^3r\, [3r^2 J_\alpha - 2r_\alpha(\mathbf{r} \cdot \mathbf{J})]r^2,$$

$$Q_{\alpha,\beta}^{(e)} = \frac{1}{2} \int d^3r\, \rho \left[r_\alpha r_\beta - \frac{1}{3}\delta_{\alpha,\beta}r^2 \right]$$
$$= \frac{1}{i2\omega} \int d^3r\, \left[r_\alpha J_\beta + r_\beta J_\alpha - \frac{2}{3}\delta_{\alpha,\beta}(\mathbf{r} \cdot \mathbf{J}) \right],$$

$$Q_{\alpha,\beta}^{(m)} = \frac{1}{3c} \int d^3r\, [\mathbf{r} \times \mathbf{J}]_\alpha r_\beta + \{\alpha \leftrightarrow \beta\},$$

$$Q_{\alpha,\beta}^{(T)} = \frac{1}{28c} \int d^3r\, [4r_\alpha r_\beta(\mathbf{r} \cdot \mathbf{J}) - 5r^2(r_\alpha J_\beta + r_\beta J_\alpha)$$
$$+ 2r^2(\mathbf{r} \cdot \mathbf{J})\delta_{\alpha,\beta}],$$

$$O_{\alpha,\beta,\gamma}^{(e)} = \frac{1}{6} \int d^3r\, \rho\, r_\alpha \left(\frac{r_\beta r_\gamma}{3} - \frac{1}{5}r^2\delta_{\beta,\gamma} \right)$$
$$+ \{\alpha \leftrightarrow \beta,\gamma\} + \{\alpha \leftrightarrow \gamma,\beta\}$$
$$= \frac{1}{i6\omega} \int d^3r\, \left[J_\alpha \left(\frac{r_\beta r_\gamma}{3} - \frac{1}{5}r^2\delta_{\beta,\gamma} \right) \right.$$
$$\left. + r_\alpha \left(\frac{J_\beta r_\gamma}{3} + \frac{r_\beta J_\gamma}{3} - \frac{2}{5}(\mathbf{r} \cdot \mathbf{J})\delta_{\beta,\gamma} \right) \right]$$
$$+ \{\alpha \leftrightarrow \beta,\gamma\} + \{\alpha \leftrightarrow \gamma,\beta\},$$

$$O_{\alpha,\beta,\gamma}^{(m)} = \frac{15}{2c} \int d^3r\, \left(r_\alpha r_\beta - \frac{r^2}{5}\delta_{\alpha,\beta} \right) \cdot [\mathbf{r} \times \mathbf{J}]_\gamma$$
$$+ \{\alpha \leftrightarrow \beta,\gamma\} + \{\alpha \leftrightarrow \gamma,\beta\}.$$

For quadrupoles and octupoles, a shorthand has been used to improve clarity. For example, $\int d^3r\, [\mathbf{r} \times \mathbf{J}]_\alpha r_\beta + \{\alpha \leftrightarrow \beta\} \equiv \int d^3r\, [\mathbf{r} \times \mathbf{J}]_\alpha r_\beta + \int d^3r\, [\mathbf{r} \times \mathbf{J}]_\beta r_\alpha$, i.e., the second term is obtained from the first term, with the exchanged positions of indices α and β. In the case of octupoles (for example),

$$\frac{1}{6} \int d^3r\, \rho\, r_\alpha \left(\frac{r_\beta r_\gamma}{3} - \frac{1}{5}r^2\delta_{\beta,\gamma} \right) + \{\alpha \leftrightarrow \beta,\gamma\} + \{\alpha \leftrightarrow \gamma,\beta\}$$

means that the second term is obtained from the first term by exchanging α and β while leaving γ untouched. The third term is, again, obtained from the first term, but this time α and γ are exchanged, while β remains untouched.

In the time-harmonic case, there is no clear difference between the conduction and displacement currents. In simulations we have used $\mathbf{J} = i\omega\epsilon_0(\tilde{\epsilon}_r - 1)\mathbf{E}$ to find the current density within the media (both metal and dielectric), from the electric field distribution $\mathbf{E}(\mathbf{r})$. The relevant quantities are ω (angular frequency), ϵ_0 (free-space permittivity), c (speed of light), and $\tilde{\epsilon}_r$ [complex-valued dielectric constant (used to describe both the dielectrics and metals)].

The spherical multipoles are related to the Cartesian multipoles through

$$Q_{1,0} = p_z, \quad Q_{1,\pm1} = (\mp p_x + i p_y)/\sqrt{2},$$

$$M_{1,0} = -m_z, \quad M_{1,\pm1} = (\pm m_x - i m_y)/\sqrt{2},$$

$$M_{1,0}^{(1)} = -m_z^{(1)}, \quad M_{1,\pm1}^{(1)} = (\pm m_x^{(1)} - i m_y^{(1)})/\sqrt{2},$$

$$T_{1,0} = T_z, \quad T_{1,\pm1} = (\mp T_x + i T_y)/\sqrt{2},$$

$$T_{1,0}^{(1)} = -T_z^{(1)}, \quad T_{1,\pm1}^{(1)} = (\pm T_x^{(1)} - i T_y^{(1)})/\sqrt{2},$$

$$Q_{2,0}^{(e)} = 3 Q_{zz}^{(e)}, \quad Q_{2,\pm1}^{(e)} = \sqrt{6}(\mp Q_{xz}^{(e)} + i Q_{yz}^{(e)}),$$

$$Q_{2,\pm2}^{(e)} = \frac{\sqrt{6}}{2}(Q_{xx}^{(e)} \mp i2 Q_{xy}^{(e)} - Q_{yy}^{(e)}),$$

$$Q_{2,0}^{(m)} = -\frac{3}{2} Q_{zz}^{(m)}, \quad Q_{2,\pm1}^{(m)} = \sqrt{\frac{3}{2}}(\pm Q_{xz}^{(m)} - i Q_{yz}^{(m)}),$$

$$Q_{2,\pm2}^{(m)} = \frac{\sqrt{6}}{4}(- Q_{xx}^{(m)} \pm i2 Q_{xy}^{(m)} + Q_{yy}^{(m)}),$$

$$Q_{2,0}^{(T)} = Q_{zz}^{(T)}, \quad Q_{2,\pm1}^{(T)} = \sqrt{\frac{2}{3}}(\mp Q_{xz}^{(T)} + i Q_{yz}^{(T)}),$$

$$Q_{2,\pm2}^{(T)} = (Q_{xx}^{(T)} \mp i2 Q_{xy}^{(T)} - Q_{yy}^{(T)})/\sqrt{6},$$

$$O_{3,0}^{(e)} = 15 O_{zzz}^{(e)},$$

$$O_{3,\pm1}^{(e)} = \mp\frac{15\sqrt{3}}{2}(O_{zzx}^{(e)} \pm i O_{yyy}^{(e)} \pm i O_{xxy}^{(e)}),$$

$$O_{3,\pm2}^{(e)} = -3\sqrt{\frac{15}{2}}(O_{zzz}^{(e)} + 2 O_{yyz}^{(e)} \pm i2 O_{xyz}^{(e)}),$$

$$O_{3,\pm3}^{(e)} = \mp\frac{3\sqrt{5}}{2}(O_{xxx}^{(e)} - 3 O_{yyx}^{(e)} \pm i O_{yyy}^{(e)} \mp i3 O_{xxy}^{(e)}),$$

$$O_{3,0}^{(m)} = - O_{zzz}^{(m)}/12,$$

$$O_{3,\pm1}^{(m)} = \pm(O_{zzx}^{(m)} \pm i O_{yyy}^{(m)} \pm i O_{xxy}^{(m)})/8\sqrt{3},$$

$$O_{3,\pm2}^{(m)} = \frac{\sqrt{2}}{8\sqrt{15}}(O_{zzz}^{(m)} + 2 O_{yyz}^{(m)} \pm i2 O_{xyz}^{(m)}),$$

$$O_{3,\pm3}^{(m)} = \pm(O_{xxx}^{(m)} - 3 O_{yyx}^{(m)} \pm i O_{yyy}^{(m)} \mp i3 O_{xxy}^{(m)})/24\sqrt{5}.$$

APPENDIX D: EXTENDED SERIES OF MULTIPOLES EXCITED IN THE CASE-STUDY METAMATERIAL

Here, we present the intensity reflected by all the multipoles in the case-study metamaterial (Fig. 3), in response to incident plane-wave radiation. Figure 6 is thus an extended version of Fig. 4(c). As one can clearly see from Fig. 6(b), the response of the case-study metamaterial is accurately captured by multipole expansion up to order k^4. Even at this level of precision, only a negligible contribution from the higher-order multipoles (i.e., $\mathbf{Q^{(m)}}, \mathbf{Q^{(T)}}, \mathbf{O^{(e)}}, \mathbf{O^{(m)}}$) is observed.

APPENDIX E: NOTATION USED FOR QUADRUPOLES AND OCTUPOLES

The expression that relates the multipole moments induced in the unit cell of the material sheet to the amplitude and phase of the emitted radiation is presented in Eq. (10) using a
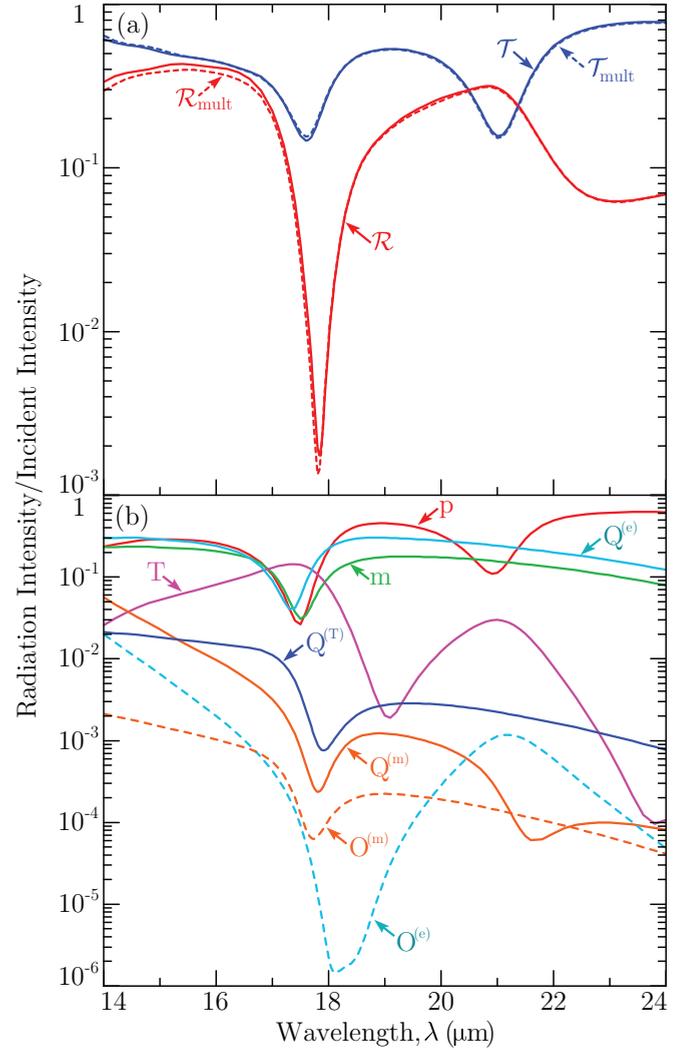

FIG. 6. (Color online) The response of the toroidal metamaterial. Extended series of multipoles that make up the response of the metamaterial from Figs. 3 and 4. (a) The transmission and reflection of the metamaterial [same data as on Fig. 4(a)]. (b) The intensity reflected by arrays of multipoles induced in the metamaterial by incident radiation [**p** (electric dipole), **m** (magnetic dipole), **T** (toroidal dipole), $\mathbf{Q^{(e)}}$ (electric quadrupole), $\mathbf{Q^{(m)}}$ (magnetic quadrupole), $\mathbf{Q^{(T)}}$ (toroidal quadrupole), $\mathbf{O^{(e)}}$ (electric octupole), $\mathbf{O^{(m)}}$ (magnetic octupole)].

coordinate-independent notation to demonstrate universality. To avoid confusion, we will clarify this notation using the coordinate frame shown in Fig. 2 with $\hat{\mathbf{R}} = \hat{\mathbf{z}}$. Using $\hat{\mathbf{x}} \cdot \hat{\mathbf{z}} = \hat{\mathbf{y}} \cdot \hat{\mathbf{z}} = 0$, $\hat{\mathbf{z}} \cdot \hat{\mathbf{z}} = 1$, $(a\hat{\mathbf{x}} + b\hat{\mathbf{y}} + c\hat{\mathbf{z}})_{\parallel} \equiv a\hat{\mathbf{x}} + b\hat{\mathbf{y}}$ and Einstein summation convention:

$$(\mathbf{Q^{(e)}} \cdot \hat{\mathbf{R}})_{\parallel} = (Q_{\alpha\beta}^{(e)} \hat{\mathbf{r}}_\alpha (\hat{\mathbf{r}} \cdot \hat{\mathbf{z}})_\beta)_{\parallel}$$

$$= (Q_{\alpha\beta}^{(e)} \hat{\mathbf{r}}_\alpha \delta_{\beta z})_{\parallel}$$

$$= (Q_{\alpha z}^{(e)} \hat{\mathbf{r}}_\alpha)_{\parallel}$$

$$= (Q_{xz}^{(e)} \hat{\mathbf{x}} + Q_{yz}^{(e)} \hat{\mathbf{y}} + Q_{zz}^{(e)} \hat{\mathbf{z}})_{\parallel}$$

$$= Q_{xz}^{(e)} \hat{\mathbf{x}} + Q_{yz}^{(e)} \hat{\mathbf{y}}.$$

For the toroidal quadrupole,

$$(\mathbf{Q^{(T)}} \cdot \hat{\mathbf{R}})_\| = Q_{xz}^{(T)} \hat{\mathbf{x}} + Q_{yz}^{(T)} \hat{\mathbf{y}}.$$

Using the conventional definition of the cross product

$$\hat{\mathbf{R}} \times (\mathbf{Q^{(m)}} \cdot \hat{\mathbf{R}})_\| = \hat{\mathbf{z}} \times \left(Q_{xz}^{(m)} \hat{\mathbf{x}} + Q_{yz}^{(m)} \hat{\mathbf{y}} \right)$$

$$= -Q_{yz}^{(m)} \hat{\mathbf{x}} + Q_{xz}^{(m)} \hat{\mathbf{y}}.$$

Similarly for the octupoles,

$$[(\mathbf{O^{(e)}} \cdot \hat{\mathbf{R}}) \cdot \hat{\mathbf{R}}]_\| = \left(O_{\alpha\beta\gamma}^{(e)} \hat{\mathbf{r}}_\alpha \delta_{\beta z} \delta_{\gamma z} \right)_\|$$

$$= O_{xzz}^{(e)} \hat{\mathbf{x}} + O_{yzz}^{(e)} \hat{\mathbf{y}},$$

$$\hat{\mathbf{R}} \times [(\mathbf{O^{(m)}} \cdot \hat{\mathbf{R}}) \cdot \hat{\mathbf{R}}]_\| = \hat{\mathbf{z}} \times \left(O_{xzz}^{(m)} \hat{\mathbf{x}} + O_{yzz}^{(m)} \hat{\mathbf{y}} \right)$$

$$= -O_{yzz}^{(m)} \hat{\mathbf{x}} + O_{xzz}^{(m)} \hat{\mathbf{y}}.$$

Thus, only two Cartesian components of each multipole moment contribute to the radiation emitted by the multipole array.

APPENDIX F: RADIATION FROM INFINITE PLANAR ARRAY WITH MARGINALLY SUBWAVELENGTH UNIT CELLS

The starting point for derivation that forms the core of this paper is the approximation in Eq. (5). In essence, we assume that the radiation from a planar array of discrete scatterers, which is given by the sum of the fields radiated by all scatterers, can be replaced with an integral over the plane of the array. In this appendix, it will be demonstrated that this approximation applies even when the unit cells of the array are only marginally smaller than the wavelength of the emitted radiation. We will demonstrate the principle using a basic example of an array of scalar wave emitters (with rectangular or square unit cells).

Consider an infinite-sized planar array of identical emitters. Assume that the complex-valued (scalar) field emitted by the single emitter at $\mathbf{r}_s$ and detected by the observer at point $\mathbf{r}_{OP}$ is given by

$$A_{k,l,m}^{(s)}(\mathbf{r}_{OP}; \mathbf{r}_s) = Y_{l,m} \left(\frac{\mathbf{r}_{OP} - \mathbf{r}_s}{|\mathbf{r}_{OP} - \mathbf{r}_s|} \right) \frac{\exp(-ik|\mathbf{r}_{OP} - \mathbf{r}_s|)}{|\mathbf{r}_{OP} - \mathbf{r}_s|},$$

where k is the wave number, and $Y_{l,m}$ are the standard spherical harmonics [58]. The total field reaching the observer at distance R away from the array will be

$$A_{k,l,m}^{(OP)}(x_{OP}, y_{OP}, R) = \sum_n A_{k,l,m}^{(s)}(x_{OP}, y_{OP}, R; \mathbf{r}_n).$$

By assuming that the array lies in the xy plane at $z = 0$ and that the observer is located above the array at $z = R$, one can replace the sum over the unit cells of the array with an integral [as in Eq. (5)] and carry out the integration (as has been shown in Appendix A) to get

$$A_{k,l,m}^{(OP)}(x_{OP}, y_{OP}, R) \approx \frac{\pi \delta_{m,0}}{ik\Delta^2} \sqrt{\frac{2l+1}{\pi}} \exp(-ikR), \quad (F1)$$

where Δ^2 is the area of the unit cell of the array.

We will now proceed to obtain the same expression without using Eq. (5). To this end, we will introduce three planes, as shown in Fig. 7: the array plane (AP) at $z = 0$, the intermediate
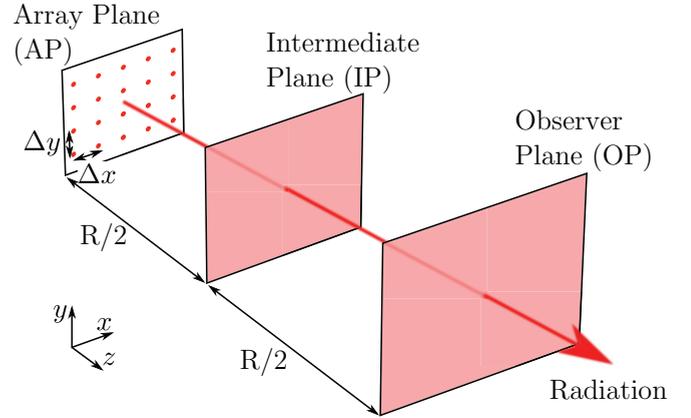

FIG. 7. (Color online) The (emitter) array plane, intermediate plane, and the observer plane used in the proof of validity of Eq. (5). The distances between the neighboring planes are $R/2$ and the lengths of the rectangular unit cells of the array are Δx and Δy.

plane (IP) at $z = R/2$, and the observer plane (OP) at $z = R$. The reason for introducing the intermediate plane is that, by placing it far enough from the array plane, we can limit our considerations to the far-field radiation patterns of the emitters. The complex-valued field at the intermediate plane will be given by the convolution of the field from a single emitter $(A^{(s)(IP)})$ and the array of two-dimensional delta functions (Ψ) that encodes the period of the (emitter) array:

$$A_{k,l,m}^{(IP)}(x, y) = \left(A_{k,l,m}^{(s)(IP)} * \Psi \right)(x, y),$$

$$\Psi(x, y) = \sum_{n,m=-\infty}^{\infty} \delta^{(2)} \left[\begin{pmatrix} x \\ y \end{pmatrix} - \begin{pmatrix} n\Delta x \\ m\Delta y \end{pmatrix} \right],$$

where Δx and Δy are the sizes of the array's unit cells along the x and y directions. Clearly, the area of the unit cell is given by $\Delta^2 = \Delta x \Delta y$.

The field reaching the observer plane can be found by Fourier propagating the field distribution at the intermediate plane up to observer plane (Sec. 3.10 from Ref. [59]):

$$A_{k,l,m}^{(OP)}(x, y) = \int df_x \int df_y$$

$$\times \exp\left[-i2\pi \left(\frac{R}{2} \right) \sqrt{\left(\frac{k}{2\pi} \right)^2 - f_x^2 - f_y^2} \right]$$

$$\times \tilde{A}_{k,l,m}^{(IP)}(f_x, f_y), \quad (F2)$$

where $\tilde{A}_{k,l,m}^{(IP)}(f_x, f_y)$ is the (spatial) Fourier transform of the field distribution at the intermediate plane. We find it by applying the convolution theorem [58,59] followed by the use of Poisson's summation formula [60] (to obtain the Fourier transform of Ψ)

$$\tilde{A}_{k,l,m}^{(IP)}(f_x, f_y) = \tilde{A}_{k,l,m}^{(s)(IP)}(f_x, f_y)$$

$$\times \frac{1}{\Delta^2} \sum_{n,m=-\infty}^{\infty} \delta^{(2)} \left[\begin{pmatrix} f_x \\ f_y \end{pmatrix} - \begin{pmatrix} n/\Delta x \\ m/\Delta y \end{pmatrix} \right],$$

$$(F3)$$

where $\tilde{A}_{k,l,m}^{(s)(IP)}(f_x, f_y)$ is the Fourier transform of the field produced by a single emitter at the intermediate plane. Substituting the above expression into Eq. (F2) and dropping the evanescent terms results in

$$A_{k,l,m}^{(OP)}(x, y) = \frac{1}{\Delta^2} \tilde{A}_{k,l,m}^{(s)(IP)}(0, 0) \exp(-ikR/2). \qquad \text{(F4)}$$

Since the unit cells are assumed to be subwavelength in size, i.e., $\lambda > \Delta x, \Delta y$ (where λ is the free-space wavelength of the emitted radiation and $k = 2\pi/\lambda$), it follows that $\frac{1}{\Delta x}, \frac{1}{\Delta y} > \frac{k}{2\pi}$. Thus, the only nonevanescent term in the sum from Eq. (F3) after substitution into Eq. (F2) is the one with $n = 0, m = 0$.

Next,

$$\tilde{A}_{k,l,m}^{(s)(IP)}(0, 0) = \int dx \int dy \, Y_{l,m}(\theta, \phi) \frac{\exp(-ikr)}{r}$$
$$= \int_{IP} d^2r \, Y_{l,m}(\theta, \phi) \frac{\exp(-ikr)}{r}. \qquad \text{(F5)}$$

Here, without the loss of generality, we assume that the position of the emitter is at the origin. Within the integral, the point (x, y) on the intermediate plane is represented as a point (r, θ, ϕ) in a spherical coordinate system [i.e., $r = r(x, y)$, etc.] with z axis pointing out of the array plane and towards the intermediate plane (see Fig. 7). The integral in Eq. (F5) is in fact very similar to $I_{l,m}$ from Appendix A. The only difference is that in case of $I_{l,m}$ the integration was carried over the array plane while the observer remained fixed. In Eq. (F5), it is the position of the "intermediate-plane observer" that is being integrated over, while the emitter, in the array plane, remains fixed. We proceed by adopting the cylindrical coordinate system (with $\rho^2 = x^2 + y^2$ and $\tan \phi = \frac{y}{x}$) for integration of Eq. (F5):

$$\tilde{A}_{k,l,m}^{(s)(IP)}(0, 0) = \int_0^{2\pi} \rho \, d\phi \int_0^\infty d\rho \, Y_{l,m}(\theta, \phi) \frac{\exp(-ikr)}{r}.$$
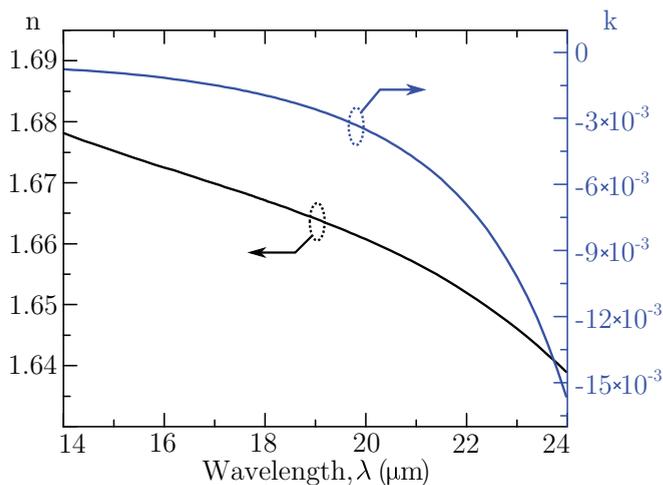

FIG. 8. (Color online) The experimentally measured refractive index of the polymer SU-8 used for simulating the case-study metamaterial. For simulations of the response of metamaterial on Fig. 3, the gold split-ring resonators were embedded into SU-8 polymer. The complex-valued refractive index of SU-8 is given by $\tilde{n} = n + ik$.
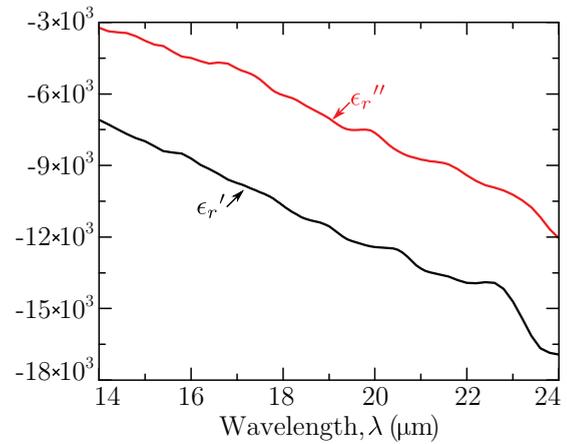

FIG. 9. (Color online) The experimentally measured dielectric constant of the gold used for simulating the case-study metamaterial. The complex-valued dielectric constant is given by $\tilde{\epsilon}_r = \epsilon_r' + i\epsilon_r''$.

As in Appendix A, $r^2 = (R/2)^2 + \rho^2$ so $r \, dr = \rho \, d\rho$ (note that the distance from AP to IP is $R/2$), and the integration over ϕ leaves only the terms with $m = 0$ (note the $\delta_{m,0}$ on the right hand side):

$$\tilde{A}_{k,l,m}^{(s)(IP)}(0, 0) = 2\pi \delta_{m,0} \int_{R/2}^\infty dr \, Y_{l,0}(\theta, 0) \exp(-ikr).$$

From this point, the integration becomes nearly identical to Appendix A, so we only give the final result

$$\tilde{A}_{k,l,m}^{(s)(IP)}(0, 0) \cong \frac{\pi \delta_{m,0}}{ik} \sqrt{\frac{2l + 1}{\pi}} \exp(-ikR/2). \qquad \text{(F6)}$$

Finally, we combine Eq. (F4) with (F6) to find

$$A_{k,l,m}^{(OP)}(x, y) \cong \frac{\pi \delta_{m,0}}{ik\Delta^2} \sqrt{\frac{2l + 1}{\pi}} \exp(-ikR), \qquad \text{(F7)}$$
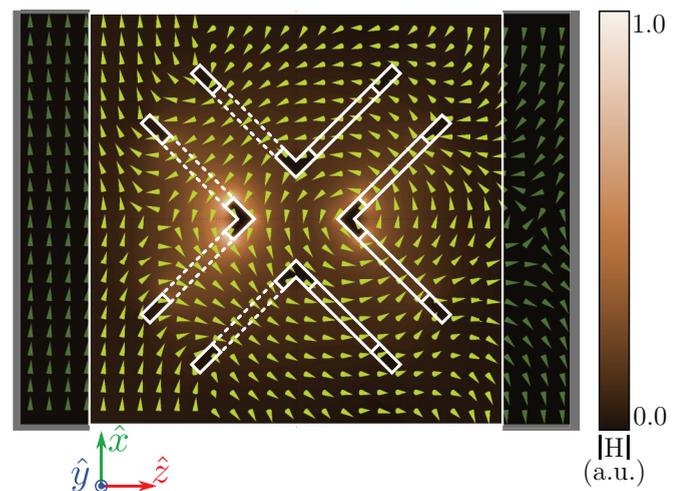

FIG. 10. (Color online) Distribution of magnetic field around the test-case metamolecule at the resonance ($\lambda = 17.4 \, \mu m$). The arrow plot shows the direction of magnetic field while the color map on the background shows the magnitude of the field. The regions outside the metamolecule have been partially screened to highlight the unit-cell boundaries.

which is the same as Eq. (F1). The conclusion is therefore that Eq. (5) is an approximation only due to dropping the evanescent waves [as in Eq. (F4)]. The size of the unit cells here is arbitrary as long as it is subwavelength. One would simply have to go to longer R in case of larger (but still subwavelength) unit cells to allow enough space for the evanescent waves to decay.

APPENDIX G: MATERIAL CONSTANTS USED IN SIMULATIONS

The material constants used for simulations have been measured and provided by Sandia National Laboratories in a private communication. An infrared variable angle spectroscopic ellipsometer (Woolam) was used to measure Ψ and Δ, from which the optical constants were derived. The same constants have been used to model the response of the previously demonstrated 3D cubic metamaterial based on SAMPL technology [54].

The refractive index of the SU-8 polymer that housed the gold split-ring resonators ($\tilde{n} = n + ik$; negative k implies losses) is shown in Fig. 8. The dielectric constant of the gold used for simulations is shown in Fig. 9 ($\tilde{\epsilon}_r = \epsilon_r' + i\epsilon_r''$; negative ϵ_r'' implies losses).

APPENDIX H: DISTRIBUTION OF MAGNETIC FIELD AROUND THE METAMOLECULE AT RESONANCE

Following the previous publications on toroidal metamaterials [11,25–31], it has become instructive to display the distribution of magnetic field around the metamolecules when the metamaterial is at toroidal resonance. The toroidal dipole may be viewed as being created by a loop of magnetization [1,4,8,9,61] (also see the schematic current distribution that gives rise to toroidal dipole shown in Fig. 1), consequently a vortex of magnetic field confined to the vicinity of the metamolecule can be taken as further evidence of strong toroidal dipole excitation. Correspondingly, we present the distribution of the magnetic field around the metamolecule of our test-case metamaterial, at the toroidal resonance, in Fig. 10.

[1] V. M. Dubovik and A. A. Cheshkov, Fiz. El. Chast. Atom. Yad. **5**, 792 (1974) [Sov. J. Particles Nucl. **5**, 318 (1975)].

[2] E. E. Radescu and G. Vaman, Phys. Rev. E **65**, 046609 (2002).

[3] T. A. Gongora and E. Ley-Koo, Rev. Mex. Fis. E **52**, 188 (2006).

[4] Ya. B. Zel'dovich, Zh. Eksp. Teor. Fiz. **33**, 1531 (1957) [Sov. Phys.–JETP **6**, 1184 (1958)].

[5] C. S. Wood *et al.*, Science **275**, 1759 (1997).

[6] W. C. Haxton and C. E. Wieman, Annu. Rev. Nucl. Part. Sci. **51**, 261 (2001).

[7] J. S. M. Ginges and V. V. Flambaum, Phys. Rep. **397**, 63 (2004).

[8] G. N. Afanasiev, J. Phys. D: Appl. Phys. **34**, 539 (2001).

[9] G. N. Afanasiev and Yu. P. Stepanovsky, J. Phys. A: Math. Gen. **28**, 4565 (1995).

[10] A. D. Boardman, K. Marinov, N. Zheludev, and V. A. Fedotov, Phys. Rev. E **72**, 036603 (2005).

[11] V. A. Fedotov, A. V. Rogacheva, V. Savinov, D. P. Tsai, and N. I. Zheludev, Sci. Rep. **3**, 2967 (2013).

[12] E. A. Marengo and R. W. Ziolkowski, Radio Sci. **37**, 19-1 (2002).

[13] S. A. Maier and H. A. Atwater, J. Appl. Phys. **98**, 011101 (2005).

[14] K. A. Willets and R. P. Van Duyne, Annu. Rev. Phys. Chem. **58**, 267 (2007).

[15] S. Lal, S. Link, and N. J. Halas, Nat. Photonics **1**, 641 (2007).

[16] M. A. Noginov *et al.*, Nature (London) **460**, 1110 (2009).

[17] H. Wang, E. C. Y. Yan, E. Borguet, and K. B. Eisenthal, Chem. Phys. Lett. **259**, 15 (1996).

[18] J. Shan, J. I. Dadap, I. Stiopkin, G. A. Reider, and T. F. Heinz, Phys. Rev. A **73**, 023819 (2006).

[19] B. K. Canfield *et al.*, J. Nonlinear Opt. Phys. Mater. **16**, 317 (2007).

[20] S. Kujala, B. K. Canfield, M. Kauranen, Y. Svirko, and J. Turunen, Opt. Express **16**, 17196 (2008).

[21] M. Zdanowicz, S. Kujala, H. Husu, and M. Kauranen, New J. Phys. **13**, 023025 (2011).

[22] M. Ren *et al.*, Adv. Mater. **23**, 5540 (2011).

[23] J. D. Jackson, *Classical Electrodynamics*, 3rd ed. (Wiley, New York, 1999).

[24] L. D. Landau and E. M. Lifschitz, *The Classical Theory of Fields*, 4th ed. (Pergamon, New York, 1975).

[25] T. Kaelberer, V. A. Fedotov, N. Papasimakis, D. P. Tsai, and N. I. Zheludev, Science **330**, 1510 (2010).

[26] Y. Fan, Z. Wei, H. Li, H. Chen, and C. M. Soukoulis, Phys. Rev. B **87**, 115417 (2013).

[27] Z.-G. Dong, P. Ni, J. Zhu, and X. Zhang, Opt. Express **20**, 13065 (2012).

[28] B. Ögüt, N. Talebi, R. Vogelgesang, W. Sigle, and P. A. van Aken, Nano Lett. **12**, 5239 (2012).

[29] Y.-W. Huang *et al.*, Opt. Express **20**, 1760 (2012).

[30] Z.-G. Dong, J. Zhu, J. Rho, J.-Q. Li, C. Lu, X. Yin, and X. Zhang, Appl. Phys. Lett. **101**, 144105 (2012).

[31] Y.-W. Huang, W. T. Chen, P. C. Wu, V. A. Fedotov, N. I. Zheludev, and D. P. Tsai, Sci. Rep. **3**, 1237 (2013).

[32] Z.-G. Dong, J. Zhu, X. Yin, J. Li, C. Lu, and X. Zhang, Phys. Rev. B **87**, 245429 (2013).

[33] A. P. Vinogradov, L. V. Panina, and A. K. Sarychev, Dokl. Akad. Nauk SSSR **234**, 530 (1989) [Sov. Phys.–Dokl. **34**, 530 (1989)].

[34] A. P. Vinogradov and A. V. Aivazyan, Phys. Rev. E **60**, 987 (1999).

[35] N. I. Zheludev, Science **328**, 582 (2010).

[36] C. M. Soukoulis and M. Wegener, Nature Photon. **5**, 523 (2011).

[37] Y. Liu and X. Zhang, Chem. Soc. Rev. **40**, 2494 (2011).

[38] C. R. Simovski, J. Opt. **13**, 013001 (2011).

[39] A. Chipouline, C. Simovski, and S. Tretyakov, Metamaterials **6**, 77 (2012).

[40] N. Engheta, W. D. Murphy, V. Rokhlin, and M. S. Vassiliou, IEEE Trans. Antennas Propag. **40**, 634 (1992).

[41] R. Coifman, V. Rokhlin, and S. Wandzura, IEEE Antennas Propag. Mag. **35**, 7 (1993).

[42] C. C. Lu and W. C. Chew, IEE Proc. H, Microw. Antennas Propag. **140**, 455 (1993).

[43] C. Craeye, IEEE Trans. Antennas Propag. **54**, 3030 (2006).

[44] W. B. Lu and T. J. Cui, J. Electromagn. Waves. Appl. **21**, 2157 (2007).

[45] R. M. Shubair and Y. L. Chow, IEEE Trans. Microwave Theory Tech. **41**, 498 (1993).

[46] A. L. Fructos, R. R. Boix, F. Mesa, and F. Medina, IEEE Trans. Antennas Propag. **56**, 3733 (2008).

[47] G. Valerio, P. Baccarelli, P. Burghignoli, and A. Galli, IEEE Trans. Antennas Propag. **55**, 1630 (2007).

[48] M. M. I. Saadoun and N. Engheta, PIER **9**, 351 (1994).

[49] A. J. Bahr and K. R. Clausig, IEEE Trans. Antennas Propag. **42**, 1592 (1994).

[50] J. B. Pendry, A. J. Holden, D. J. Robbins, and W. J. Stewart, IEEE Trans. Microwave Theory Tech. **47**, 2075 (1999).

[51] C. Rockstuhl *et al.*, Opt. Express **15**, 8871 (2007).

[52] J. C.-E. Sten and D. Sjöberg, PIER B **35**, 187 (2011).

[53] A. I. Akhiezer and V. B. Berestetskii, *Quantum Electrodynamics*, 2nd ed. (Interscience, New York, 1965).

[54] D. B. Bruckel *et al.*, Adv. Mater. **22**, 5053 (2010).

[55] J. Zhang, K. F. MacDonald, and N. I. Zheludev, Light Sci. Appl. **1**, e18 (2012).

[56] X. Fang, M. L. Tseng, J.-Y. Ou, K. F. MacDonald, D. P. Tsai, and N. I. Zheludev, Appl. Phys. Lett. **104**, 141102 (2014).

[57] M. Abramowitz and I. A. Stegun, *Handbook of Mathematical Functions with Forumulas, Graphs, and Mathematical Tables*, 10th ed. (Dover, New York, 1972).

[58] G. B. Arfken and H. J. Weber, *Mathematical Methods for Physicists*, 5th ed. (Harcourt/Academic, Oxford, 2001).

[59] J. W. Goodman, *Introduction to Fourier Optics*, 2nd ed. (McGraw-Hill, New York, 1996).

[60] M. J. Lighthill, *An Introduction to Fourier Analysis and Generalised Functions* (Cambridge University Press, London, 1964).

[61] V. M. Dubovik and V. V. Tugushev, Phys. Rep. **187**, 145 (1990).